Journal of Marine Science and Application
https://doi.org/10.1007/s11804-020-00136-4

Ultimate Compressive Strength Computational Modelling for Stiffened Plate Panels with Non-Uniform Thickness

Hyun Ho Lee[1] **and Jeom Kee Paik**[1,2,3]

Received: 08-May-2020/Accepted: 01-Aug-2020

Abstract
The aim of this paper is to develop computational models for the ultimate compressive strength analysis of stiffened plate panels with non-uniform thickness. Modelling welding-induced initial deformations and residual stresses were presented with the measured data. Three methods, i.e., ANSYS finite element method, ALPS/SPINE incremental Galerkin method and ALPS/ULSAP analytical method were employed together with existing test database obtained from a full-scale collapse testing of steel stiffened plate structures. Sensitivity study was conducted with varying the difference in plate thickness to define a representative (equivalent) thickness for plate panels with non-uniform thickness. Guidelines are provided for structural modelling to compute the ultimate compressive strength of plate panels with variable thickness.

Keywords Ultimate compressive strength • Steel stiffened plate structures • Non-uniform plate thickness • ANSYS finite element method • ALPS/SPINE incremental Galerkin method • ALPS/ULSAP analytical method

Article Highlights
- Computational models for the ultimate compressive strength analysis of stiffened plate panels with non-uniform thickness
- Application of the three methods of ANSYS finite element method, ALPS/SPINE incremental Galerkin method and ALPS/ULSAP analytical method
- Validation of the computational models by a comparison with full-scale physical test
- Guidelines for structural modelling to compute the ultimate compressive strength of stiffened plate panels with non-uniform thickness

1 Introduction

Plate panels are used in naval, offshore, mechanical, aerospace and civil engineering structures as primary strength parts of ships, ship-shaped offshore installations, fuselages, box-girder cranes, and bridges. They are usually designed and built with a uniform thickness over the plating, but non-uniform thickness is sometimes allocated to fulfill practical design requirements (Zenkour 2003, Lee et al. 2019, Tash and Neya 2020).

During the past several decades, the emphasis on structural design has moved from the allowable stress design to the limit state design because the latter approach makes possible a rigorously designed, yet economical, structure that directly takes into consideration the various relevant modes of failure (Paik 2018). Furthermore, limit states are key criteria within the framework of quantitative risk assessment and management which is now recognized to be the best way to effectively manage extreme conditions and accidents associated with the volatile, uncertain, complex and ambiguous environments at every stage of design, construction, operation and decommissioining of structures and infrastructure, and ultimately resolve such challenges (Paik 2020).

✉Jeom Kee Paik
j.paik@ucl.ac.uk

1 Department of Naval Architecture and Ocean Engineering, Pusan National University, Busan, South Korea
2 The Korea Ship and Offshore Research Institute (Lloyd's Register Foundation Research Centre of Excellence), Pusan National University, Busan, South Korea
3 Department of Mechanical Engineering, University College London, London, UK

A limit state is formally defined by the description of a condition for which a particular structural member of an entire structure would fail to perform the function designated beforehand, and four types of limit states are relevant for structures, namely the servicebility limit state (SLS), the ultimate limit state (ULS), the fatigue limit state (FLS), and the accidental limit state (ALS) from the viewpoint of structural design (Paik 2018). This paper deals with the the ultimate limit state of a steel stiffened plate structure under uniaxial compresive loads.

A number of useful studies on the ultimate strength of plate panels for marine applications are found in the literature (Abdussamie et al. 2018, Benson et al. 2011, Gannon et al. 2013, 2016, Iijima et al. 2015, Jagite et al. 2019, 2020, Khan and Zhang 2011, Khedmati et al. 2014, 2016, Kim et al. 2009, 2015, Kumar et al. 2009, Lee and Paik 2020, Magoga and Flockhart 2014, Ozguc et al. 2006, Paik 2007, Paik et al. 2013, Rahbar-Ranji and Zarookoan 2015, Ringsberg et al. 2018, Shi and Gao 2020, Shi and Wang 2012, Zhang 2016, Wang et al. 2009). For plate panels of engineering structures with variable or non-uniform thickness, the structural responses should be characterised by taking into account the effects of variable thickness. Zenkour (2003) and Tash and Neya (2020) studied the bending behavior of transversely isotropic thick rectangular plates with variable thickness. de Faria and de Almeida (2002) and Le-Manh et al. (2017) studied buckling of composite plates with variable thickness. Zhang et al. (2018) studied buckling of egg-shaped shells with variable thickness under external pressure loads. However, no studies on the ultimate strength of isotropic plate panels with variable or non-uniform thickness are found in the literature.

The aim of the present paper is to contribute to developing computational models for the ultimate compressive strength analysis of steel stiffened plate panels with non-uniform thickness. The paper is a sequel to the articles of Paik et al. (2020a,b,c,d,e) that dealt with full-scale progressive collapse testing on steel stiffened plate structures under various circumstances such as low temperature or fires.

2 A target stiffened plate panel

A stiffened plate panel subjected to axial compressive loads is considered as shown in Figure 1. The panel is composed of three bays. The plating of outer two bays has a same thickness of t. However, the thickness for a half of the plating in the central bay is t_1 and t_2. The target plate panel with $t = t_1 = t_2$ was fabricated with the framework of full-scale collapse tests (Paik 2020a, b, c, d and e), where the bottom plate panels of a containership carrying 1900 TEU were a reference.

The panel has four longitudinal stiffeners and two transverse frames with T-type as shown in Figure 2. The dimensions of longitudinal stiffeners in outer two bays are the same, but they are larger than from those in the central bay. This means that the outer two bays may not buckle until the central bay reaches the ultimate limit state. Table 1 presents the dimensions of the plate panel. The plate panel is fixed along the loaded edges (i.e., left and right ends), but the unloaded edges are simply supported, i.e., with the constraints of lateral deformation but free rotation. Also, the unloaded edges are allowed to move in-plane freely, implying that they may not keep straight as the plate panel deflects due to buckling.

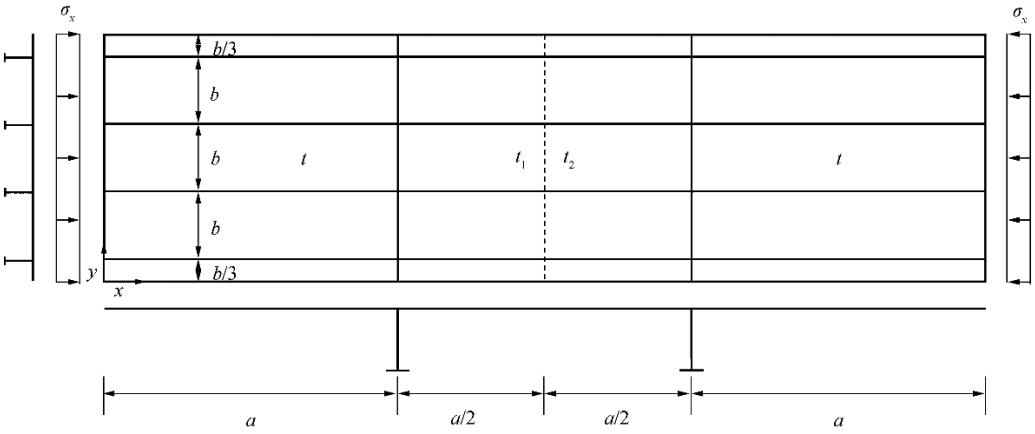

Figure 1 A stiffened plate panel

Table 1 Dimensions of the target plate panel Unit: mm

a	b	Plate thickness			Longitudinal stiffener								Transverse frame			
		t	t_1	t_2	Outer bays				Central bay				h_{wy}	t_{wy}	b_{fy}	t_{fy}
					h_{wx}	t_{wx}	b_{fx}	t_{fx}	h_{wx}	t_{wx}	b_{fx}	t_{fx}				
3150	720	10	Vary	Vary	290	20	90	10	290	10	90	10	665	10	150	10

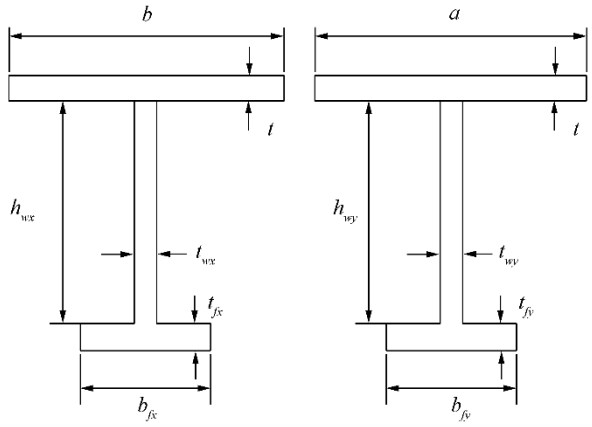

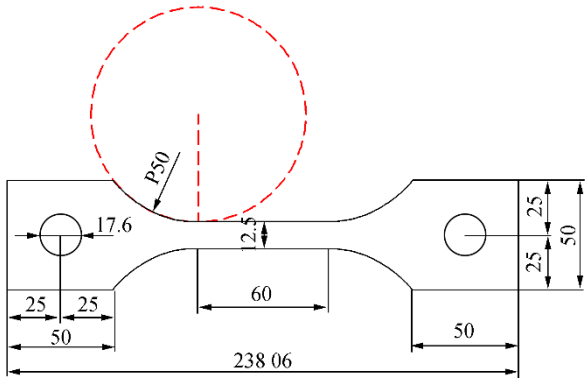

(a) Dimension of the tensile test specimen

Figure 2 T-type support members in the x and y directions

(b) Specimen with extensometer

(c) Specimen after completing tensile test

Figure 3 Specimen of material used for the structure before and after tensile coupon tests

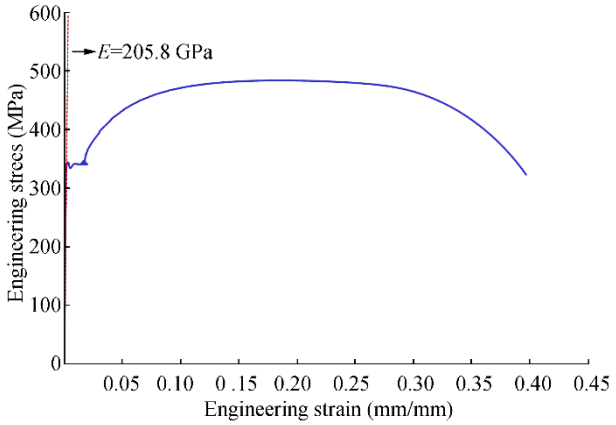

Figure 4 Engineering stress versus engineering strain curve of the AH32 steel

The plate panel is made of high tensile steel with grade AH32. To define the mechanical properties of the material the tensile coupon tests were conducted with specimens made in compliance with ASTM E8 (ASTM 2011), as shown in Figure 3. Figure 4 shows one of typical engineering stress-engineering strain curves of the material obtained from tensile coupon tests with multiple specimens. Table 2 provides the mechanical properties of the AH32 steel.

Table 2 Mechanical properties of the AH32 steel obtained from the tensile coupon tests.

Grade	E (GPa)	σ_Y (MPa)	σ_T (MPa)	ν	ε_f (%)
AH32	205.8	331	483	0.3	40.0

Notes: E is the elastic modulus, σ_Y is the yield strength, σ_T is the ultimate tensile strength, ν is the assumed Poisson's ratio, and ε_f is the fracture strain

3 Modelling of weld-fabrication induced initial imperfections of the plate panel

The plate panel with $t = t_1 = t_2$ =10 mm was fabricated in a shipyard in Busan, South Korea which builds small and medium sized merchant and patrol ships. The technology of welding was exactly the same as used for fabrication of real ship structures. The flux-cored arc welding (FCAW) technique was applied in accordance with the welding procedure specification (WPS) requirements as indicated in Table 3. As per the welding requirements of DNVGL (2017), the penetration of welding was fully achieved with a leg length of 7 mm as shown in Figure 5. Figure 6 shows the plate panel after fabrication was completed in the shipyard.

Table 3 Welding parameters of the actual welding process and welding procedure specifications

Leg length, L_w (mm)	Welding parameter				
	Weld condition	Current (A)	Voltage (V)	Speed (cm/min)	Heat input (KJ/cm)
7	WPS	225-275	23-32	24-34	7-18
	Real condition	260	28	30	14.56

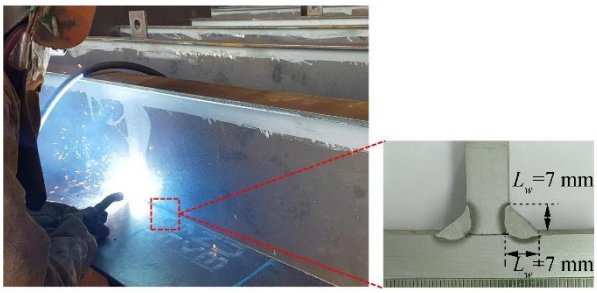

Figure 5 Full penetration of welds with a leg length of 7 mmm

Figure 6 The plate panel after completing of fabrication in the shipyard

3.1 Modelling of the plate initial deflection

A 3D scanner was used to measure the welding-induced initial deformations for plating and support members. For details of the initial deformation measurements together with the thermal-elastic-plastic large deformation finite element method computations, Yi et al. (2020a) is referred to. Figure 7 presents the welding-induced initial deflection of plating in the plate length and breadth directions. It is seen that not only plating but also transverse frames were deflected by welding, where the relative maximum of the plate initial deflection was found to be 1.73 mm based on the measured data. On the other hand, the maximum sideways deformation of longitudinal stiffeners was 0.42 mm which is $0.000133a$. The web initial deflections for both longitudinal stiffeners and transverse frames were negligibly small.

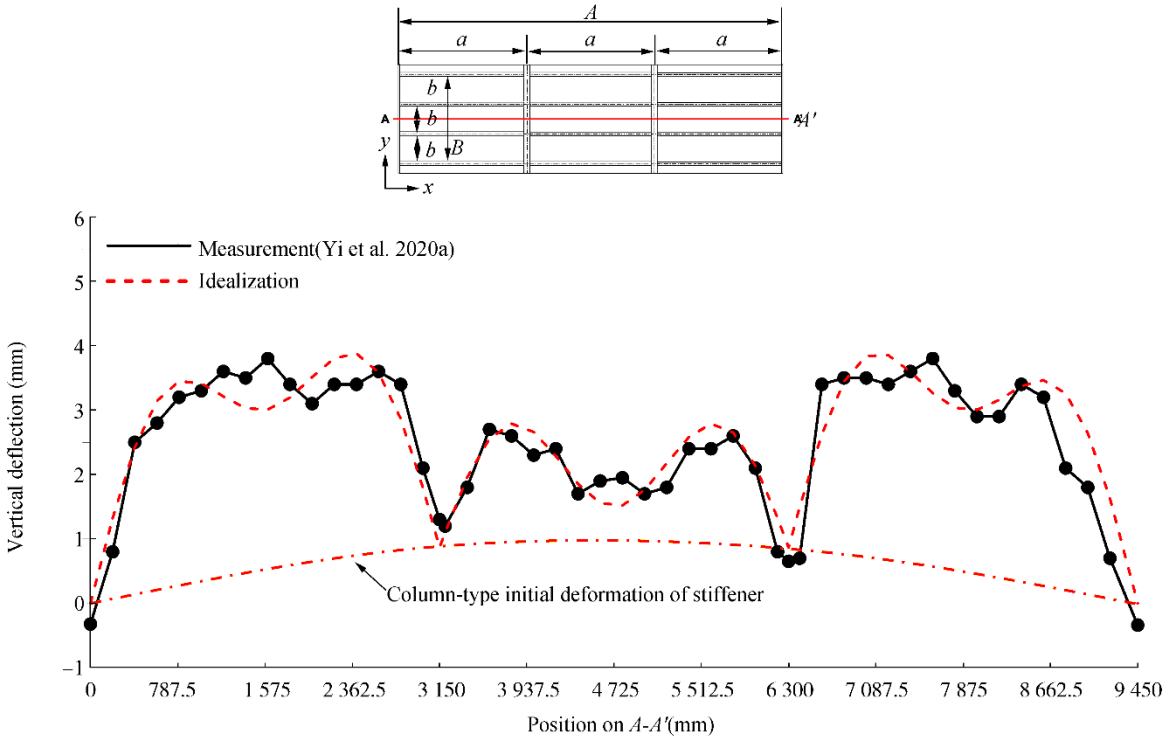

(a) Welding-induced initial deflection of plating in the plate length direction (along the A-A' section)

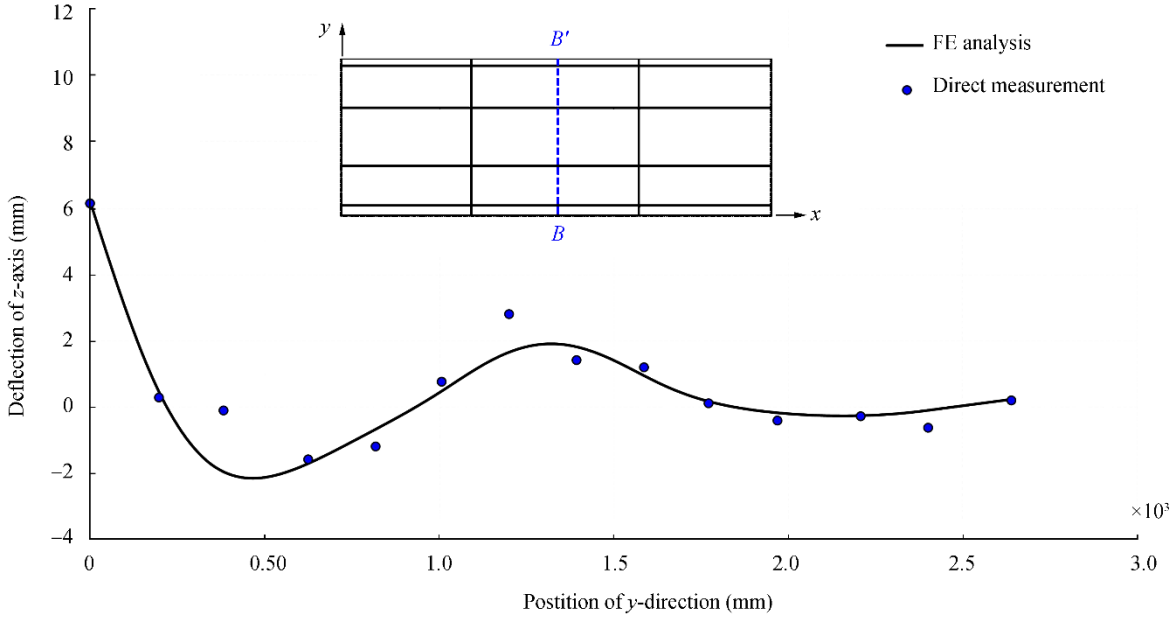

(b) Welding-induced initial deflection of plating in the plate breadth direction (along the B-B' section)

Figure 7 Comparison between direct measurements and numerical computations of plate initial deflections (Yi et al. 2020a)

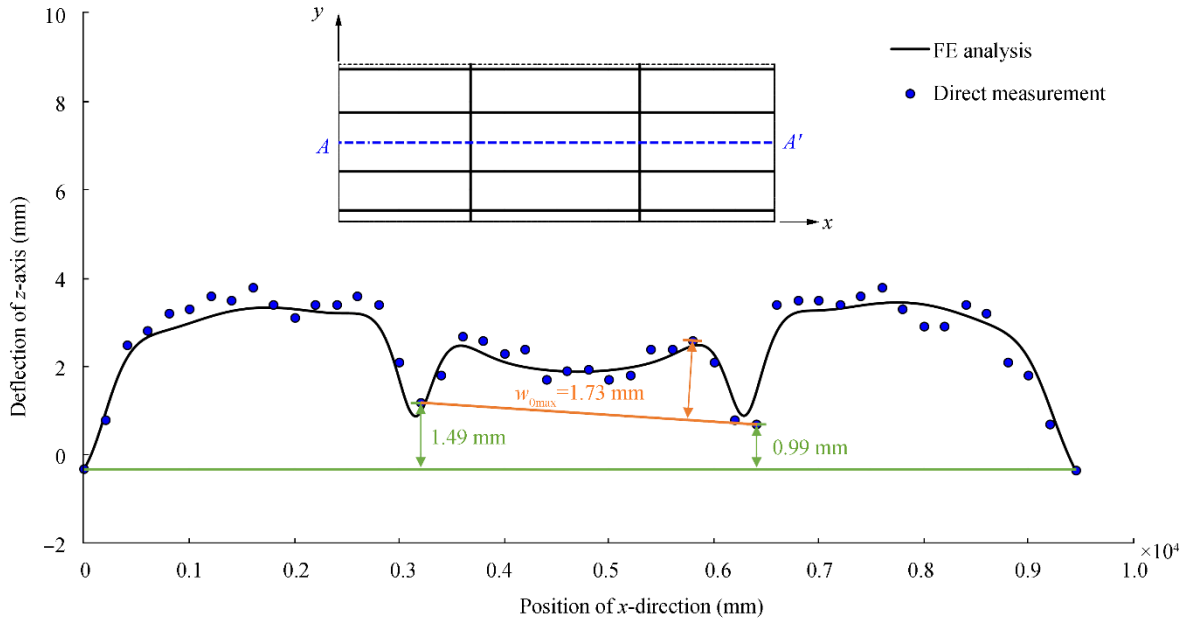

Figure 8 The maximum deflections of plating and transverse frames

The shape of the plate initial deflection is the so-called hungry horse's back type. In this case, the plate initial deflection of the central bay panel but excluding the unloaded side plates may be formulated by the following Fourier series equation (Paik 2018) where only a single half-wave between longitudinal stiffeners is allocated in the plate breadth direction.

$$\frac{w_0}{w_{o\max}} = \sum_{i=1}^{11} B_{oi3} \sin\frac{i\pi x}{a} \sin\frac{3\pi y}{B} \tag{1}$$

where w_0 is the plate initial deflection function, $w_{0\max}$ is the maximum plate initial deflection, $B = 3b$ is the breadth of the panel and B_{0i3} is the coefficients of the plate initial deflection.

The buckling mode of plating is defined as an integer satisfying the following equation.

$$\frac{a}{b} \le \sqrt{m(m+1)} \tag{2}$$

where m is the buckling half-wave number. With a = 3150 mm and b = 720 mm, $m = 4$ is determined.

Equation (1) may be simplified with only the buckling component as follows:

$$\frac{w_0}{w_{o\max}} = B_{o43} \sin\frac{4\pi x}{a} \sin\frac{3\pi y}{B} \tag{3}$$

where B_{043} is the buckling component of the plate initial deflection function which may be taken as B_{043} = 0.0259 (Paik 2018) as far as the hungry horse's back shape is applied.

3.2 Modelling of the residual stresses

As both longitudinal stiffeners and transverse frames are attached to the plating by welding, residual stresses must be developed in the two directions as shown in Figure 9. Tensile residual stresses are developed in the heat affected zone, and compressive residual stresses are developed in the middle of plating to fulfil the equilibrium condition between internal forces. The X-ray diffraction (XRD) method was used to measure welding-induced residual stresses in the plate panel. Details of the residual stress measurements together with the thermal elastic-plastic finite element method computations and the simple formula estimations are presented in Yi et al. (2020b). Figure 10 shows the comparison of welding-induced residual stresses between direct measurement, finite element method computations and simple formula estimations.

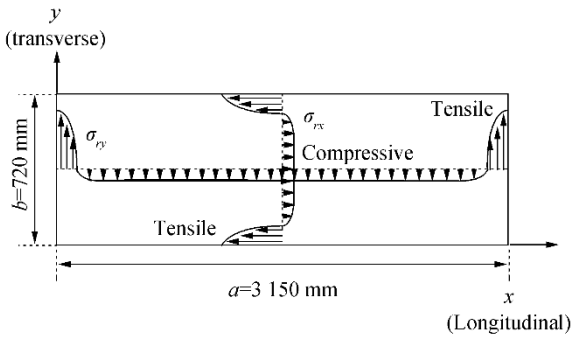

Figure 9 Distribution of welding-induced residual stresses in the two directions

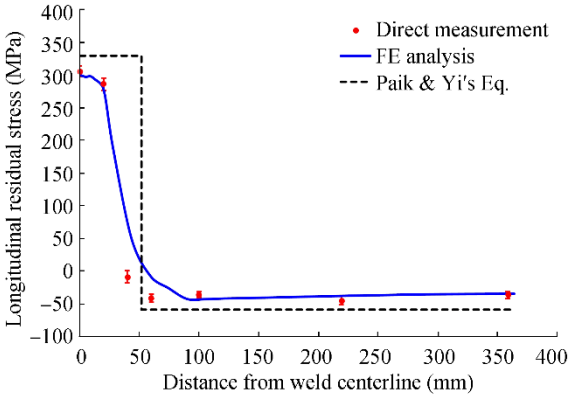

(a)

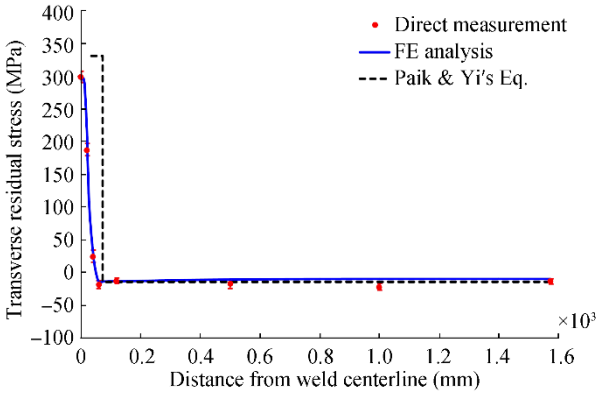

(b)

Figure 10 A comparison of welding-induced residual stresses between direct measurements, numerical predictions and simple formula estimations (a) in the longitudinal stiffener direction and (b) in the transverse frame direction.

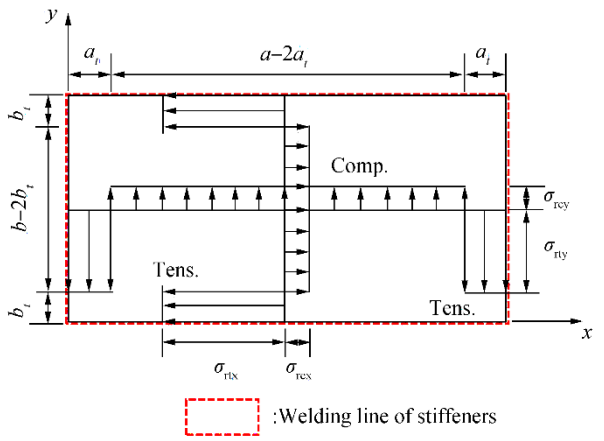

Figure 11 Idealisation of the welding-induced residual stresses in a plate

The distribution of welding-induced residual stresses is often modelled as rectangular blocks of tensile and compressive residual stresses as shown in Figure 11. For welded steel plates, the welding-induced residual stresses may be estimated by the following procedure (Paik 2018).

From the equilibrium condition, the compressive residual stresses are obtained as follows:

$$\sigma_{rcx} = \frac{2b_t}{2b_t - b}\sigma_{rtx} \tag{4a}$$

$$\sigma_{rcy} = \frac{2a_t}{2a_t - a}\sigma_{rty} \tag{4b}$$

where b_t and a_t are the breadth of tensile residual stress block in the plate breadth or length direction, respectively, σ_{rtx}, σ_{rty} are the magnitude of tensile residual stress block in the plate length or breadth direction, respectively, σ_{rcx}, σ_{rcy} are the magnitude of compressive residual stress block in the plate length or breadth direction, respectively, a is the plate length (spacing between transverse frames), and b is the plate breadth (spacing between longitudinal stiffeners). σ_{rtx} and σ_{rty} are approximately equal to σ_Y (material yield strength) for structural steels.

Equation (4) indicates that the compressive residual stresses can be estimated once the breadths of tensile residual stress blocks are defined. Empirical formulations of b_t and a_t were developed as a function of the weld leg length L_w as follows (Paik 2018):

$$b_t = c_1 \times L_w + c_2 \tag{5}$$

where, $c_1 = -0.4562 \times \beta_x^2 + 4.1994 \times \beta_x + 2.6354$,

$c_2 = 1.1352 \times \beta_x^2 - 4.3185 \times \beta_x - 11.1750$

and $\beta_x = \frac{b}{t}\sqrt{\frac{\sigma_Y}{E}}$.

$$a_t = d_1 \times L_w + d_2 \tag{6}$$

where, $d_1 = -0.0399 \times \beta_y^2 + 2.0087 \times \beta_y + 8.7880$,

$d_2 = 0.1042 \times \beta_y^2 - 4.8575 \times \beta_y - 17.7950$ and

$\beta_y = \frac{a}{t}\sqrt{\frac{\sigma_Y}{E}}$.

Using Equations (4) – (6), the magnitude of compressive residual stresses in the longitudinal and transverse directions can be estimated. The yield strength of the AH32 steel is 331 MPa and thus $\sigma_Y = \sigma_{rtx} = \sigma_{rty}$ = 331 MPa is taken. Also, the leg length for the applied weld condition is L_w = 7 mm. Therefore, the slenderness ratios are calculated as $\beta_x = 2.88$ and $\beta_y = 12.63$. Equations (5) and (6) provide the breadths of tensile residual stress blocks as follows:

$$c_1 = -0.4562 \times \beta_x^2 + 4.1994 \times \beta_x + 2.6354$$
$$= -0.4562 \times 2.88^2 + 4.1994 \times 2.88 + 2.6354 = 10.9575$$
$$c_2 = 1.1352 \times \beta_x^2 - 4.3185 \times \beta_x - 11.1750$$
$$= 1.1352 \times 2.88^2 - 4.3185 \times 2.88 - 11.1750 = -14.1797$$
$$b_t = c_1 \times L_w + c_2 = 51.5655 \text{ mm}$$
$$d_1 = -0.0399 \times \beta_y^2 + 2.0087 \times \beta_y + 8.7880$$
$$= -0.0399 \times 12.63^2 + 2.0087 \times 12.63 + 8.7880 = 27.7960$$
$$d_2 = 0.1042 \times \beta_y^2 - 4.8575 \times \beta_y - 17.7950$$
$$= 0.1042 \times 12.63^2 - 4.8575 \times 12.63 - 17.7950 = -95.7883$$
$$a_t = d_1 \times L_w + d_2 = 70.9877 \text{ mm}$$

The compressive residual stresses in the longitudinal and transverse directions are estimated from Equation (4) as follows:

σ_{rcx} = -55.34 MPa, σ_{rcy} = -14.92 MPa

Figure 10 presents the validity of the procedure to estimate the welding-induced residual stresses in the plate panel.

4 Computational models

4.1 ALPS/ULSAP (2020) analytical method

The primary modes of overall failure for a stiffened plate structure are categorized into the following six types (Paik 2018):

- Mode I: Overall collapse of plating and stiffeners as a unit
- Mode II: Plate collapse without distinct failure of stiffeners
- Mode III: Beam-column type collapse
- Mode IV: Collapse by local web buckling of stiffener

- Mode V: Collapse by lateral-torsional buckling (tripping) of stiffener
- Mode VI: Gross yielding

Some collapse modes may in some cases interact and occur simultaneously, but it is typically considered that the collapse of the stiffened panels occurs at the lowest value among the various ultimate loads calculated when considering each of the above-mentioned six collapse patterns separately. Details of the ULS computations for each of the six collapse modes are found in Paik (2018), and they have been implemented into the ALPS/ULSAP program (2020). This method accommodates the application of combined load components such as biaxial compression / tension, biaxial in-plane bending, edge shear, and lateral pressure loads. The effects of welding-induced initial imperfections in the form of initial deformations and residual stresses are taken into account.

With ALPS/ULSAP, only the plate panel of the central bay which is assumed to be simply supported is taken as the extent of the analysis as shown in Figure 12. Also, only the buckling mode of the plate initial deflection is considered using Equation (3). The measured values of the biaxial residual stresses are used but with the idealised distribution as shown in Figure 12. It is assumed that welding-induced residual stresses of longitudinal stiffeners are not considered. The column type initial deflection of longitudinal stiffeners is assumed to be $0.0015a$. The material follows the elastic-perfectly plastic model without considering strain-hardening effect.

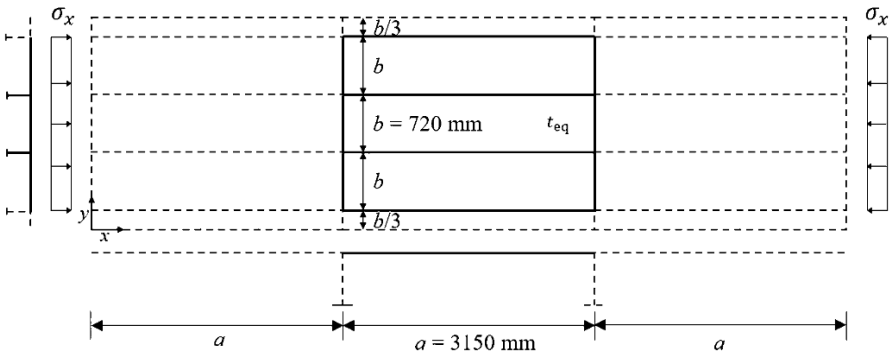

Figure 12 Extent of the ALPS/ULSAP and ALPS/SPINE analyses

A total of four cases with varying the thicknesses t_1 and t_2 are studied while the average value of them is kept constant at $t = \frac{t_1 + t_2}{2}$ as indicated in Table 4. For the ALPS/ULSAP analysis, the smaller value of the plate thickness, i.e., with $t_{eq} = t_2$ when $t_1 \geq t_2$ is used so that the ultimate strength is computed for the plate panel with a uniform thickness of $t_{eq} = t_2$.

Table 4 Variation of the plate thickness

Case	t (mm)	t_1 (mm)	t_2 (mm)	$t_{eq} = t_2$ (mm)
1	10.0	10.0	10.0	10.0
2	10.0	10.5	9.5	9.5
3	10.0	11.0	9.0	9.0
4	10.0	11.5	8.5	8.5

4.2 ALPS/SPINE (2020) incremental Galerkin method

The incremental Galerkin method developed by Paik et al. (2001) and Paik and Lee (2005) is a semi-analytical method for computing the elastic-plastic large-deflection behavior of steel or aluminum plates and stiffened panels up to their ultimate limit state (ULS). This method is designed to accommodate the geometric nonlinearity associated with buckling via an analytical procedure, whereas a numerical procedure accounts for the material nonlinearity associated with plasticity (Paik 2018). The method is unique in its use to analytically formulate the incremental forms of nonlinear governing differential equations for elastic large-deflection plate theory. After solving these incremental governing differential equations using the Galerkin approach (Fletcher 1984), a set of easily solved linear first-order simultaneous equations for the unknowns is obtained, which facilitates a reduction in the computational effort.

It is normally difficult, but not impossible, to formulate the nonlinear governing differential equations to represent both geometric and material nonlinearities for plates and stiffened panels. A major source of difficulty is that an analytical treatment of plasticity with increases in the applied loads is quite cumbersome. An easier alternative is to deal with the progress of the plasticity numerically. The benefits of this method are to provide excellent solution accuracy with great savings in computational effort and to handle in the analysis the combined loading for all potential load components, including biaxial compression or tension, biaxial in-plane bending, edge shear, and lateral pressure loads. The effects of initial imperfections in the form of initial deflection and welding-induced residual stresses are also considered. The present theory can be applied to both steel and aluminum plate panels. Details of the IGM theory and applied examples described in Paik (2018) have been implemented into the ALPS/SPINE program.

In the following, some of the more important basic hypotheses used to formulate the incremental Galerkin method for computation of the elastic-plastic large-deflection behavior of plate and stiffened panels are described (Paik 2018).

The plate panel is made of isotropic homogeneous steel or aluminum alloys with a Young's modulus of E and a Poisson's ratio of ν . For a stiffened panel, Young's modulus of the plate part between stiffeners is the same as that of the stiffeners, but the yield stress of the plate part can differ from that of the stiffeners.

1) The length and breadth of the plate are a and b , respectively, as shown in Figure 13(a). The plate thickness is t .
2) The spacing of the stiffeners or the breadth of the plating between stiffeners can differ as shown in Figure 13(b).

3) The material follows the elastic-perfectly plastic model without considering the strain-hardening effect.
4) The edge of the panel can be simply supported, clamped, or some combination of the two.
5) The panel is normally subjected to combined loads. Several potential load components act on the panel: biaxial compression or tension, edge shear, biaxial in-plane bending moment, and lateral pressure loads, as shown in Figure 14.
6) The applied loads are increased incrementally.
7) The shape of the initial deflection in the plate panel is normally complex, but it can be expressed with a Fourier series function. For a stiffened panel, the plate part between stiffeners may have the same set of local plate initial deflections, whereas the stiffeners may have a different set of global column-type initial deflections.
8) Due to the welding along the panel edges and at the intersections between the lower part of the stiffener web and parent plate, the panel has welding-induced residual stresses. These can develop in the plate part in both x and y directions, as welding is normally carried out in these two directions. As shown in Figure 15, the distribution of welding-induced residual stresses for the plate part between stiffeners is idealized to be composed of two stress blocks, i.e., compressive and tensile residual stress blocks. It is assumed that the stiffener webs have uniform compressive residual stresses "equivalent" to that shown in Figure 14.
9) For evaluation of the plasticity, it is assumed that the panel is composed of a number of membrane fibers in the x and y directions. Each membrane fiber is considered to have a number of layers in the z direction, as shown in Figure 15.
10) It is recognized that the strength of welded aluminum alloys in the softened zone may be recovered by natural aging over a period of time, but the ultimate strength of welded aluminum alloy panels may be reduced by softening phenomenon in the heat-affected zone as far as the material strength is not recovered. The effect of softening is accounted for using the technique noted in item 9 above.

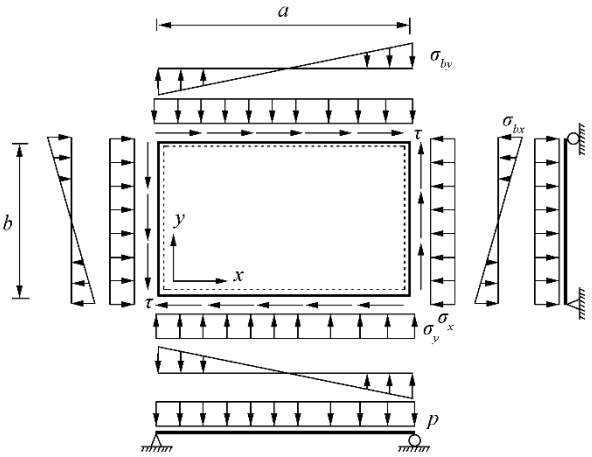

(a)

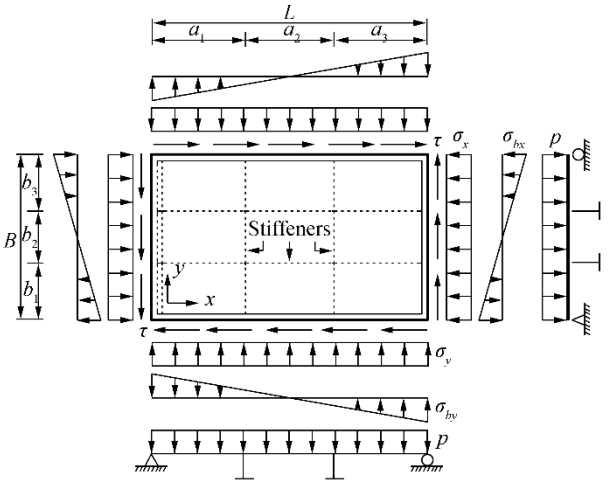

(b)

Figure 13 Application of combined in-plane and out-of-plane loads in (a) a plate, (b) a stiffened panel.

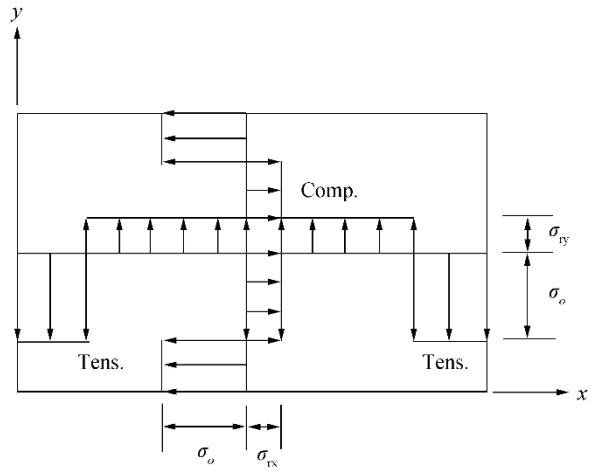

(a)

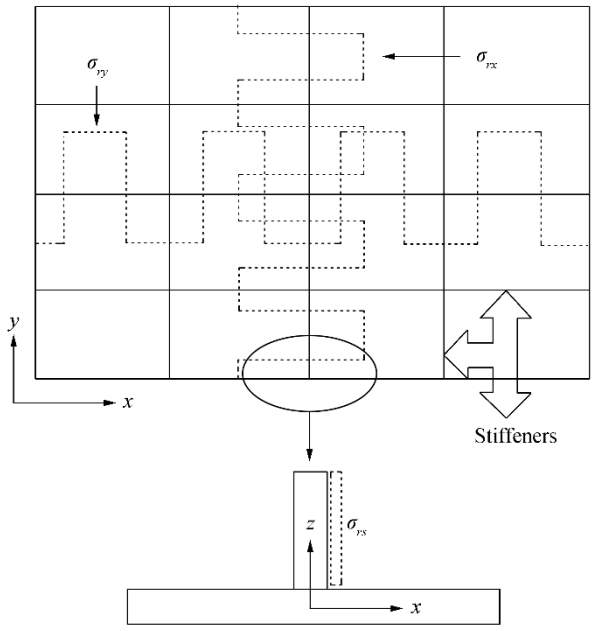

(b)

Figure 14 Idealized welding-induced residual stress distribution inside (a) the plating, (b) the stiffeners

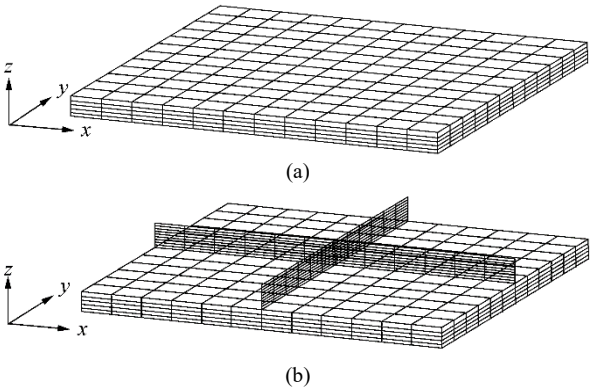

Figure 15 Example subdivision of mesh regions used for treatment of plasticity for (a) a plate, (b) a stiffened panel (note that geometric nonlinearity is handled analytically)

The extent of the ALPS/SPINE analysis was the same as that of the ALPS/ULSAP analysis as shown in Figure 12. The plate initial deflection was assumed as follows:

$$\frac{w_0}{w_{o\max}} = \sin\frac{\pi x}{a}\sin\frac{3\pi y}{B} + B_{o43}\sin\frac{4\pi x}{a}\sin\frac{3\pi y}{B} \tag{8}$$

Furthermore, the added plate deflection under applied loads was assumed to follow the equation.

$$w = \sum_{i=1}^{9} A_{i3}\sin\frac{i\pi x}{a}\sin\frac{3\pi y}{B} \tag{9}$$

where w is the added plate deflection and A_{i3} is the amplitude of added deflection components.

Similar to the ALPS/ULSAP model, the measured values of the biaxial residual stresses were used but with the idealised distribution as shown in Figure 12. It was assumed that welding-induced residual stresses of longitudinal stiffeners were not considered. The column type initial deflection of longitudinal stiffeners was assumed to be 0.0015a. Again, a total of four cases including one case with uniform plate thickness were studied as indicated Table 4. The smaller value of the plate thickness, i.e., with $t_{eq} = t_2$ when $t_1 \geq t_2$ was applied for the ALPS/SPINE analysis.

4.3 ANSYS finite element method

The entire structure was taken as the extent of the analysis as shown in Figure 16. Only plate elements (with an aspect ratio of unity if possible) were used to model not only plating but also support members including both webs and flanges. The mesh size was taken as b/10 for plating. Two elements (with one element at each side of T-bar) were used for the flange of longitudinal stiffener, and four elements (with two elements at each side of T-bar) were used for the flange of transverse frame.

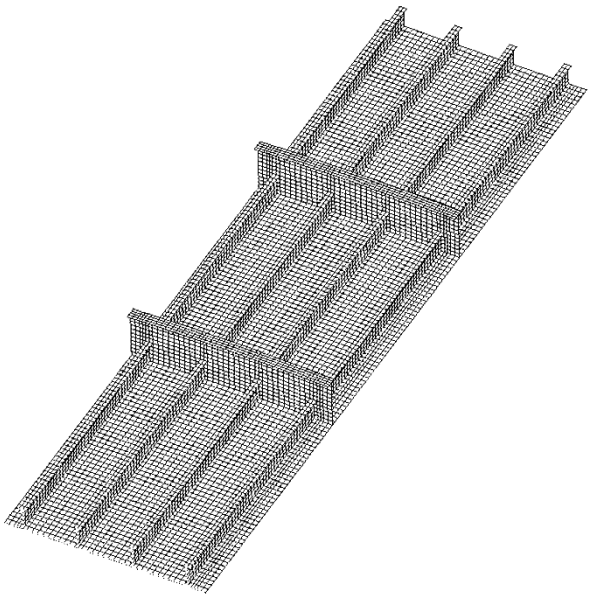

Figure 16 Extent of the ANSYS finite element method analysis.

The plate initial deflection was assumed with only the buckling mode of Equation (3). The measured initial deflection of transverse frames shown in Figure 8 were directly considered. The measured residual stresses were included in the modelling. The maximum sideways deformation of longitudinal stiffeners was applied, and the web initial deflections of both longitudinal stiffeners and transverse frames were neglected. In contrast to ALPS/ULSAP and ALPS/SPINE analyses, the actual plate thicknesses of t_1 and t_2 were directly included in the ANSYS modelling, while a total of four cases were studied as indicated in Table 4. The elastic-perfectly plastic material model was applied for the ANSYS analysis. Figure 17 shows the finite element model of the tested structure. Figure 18 shows the boundary condition applied for the ANSYS finite element analysis which was the same as for the tested structure.

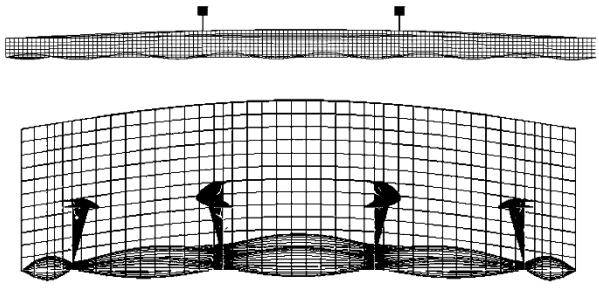

Figure 17 Modelling of initial deformations in the plate and support members

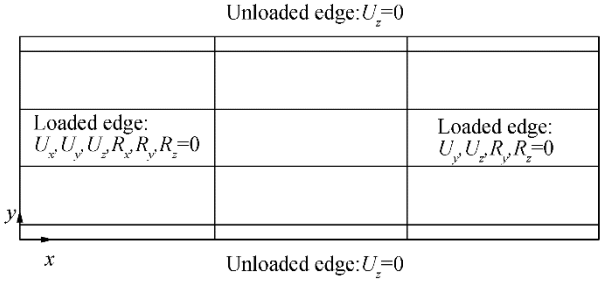

Figure 18 Boudanry condition applied for the ANSYS finite element method analysis

5 Computed results and discussion

Figure 19 shows the applied compressive load versus axial shortening curves of the plate panel with $t = t_1 = t_2$ = 10 mm, where unloaded edges are allowed to move in-plane freely without keeping straight. To investigate the effect of the straight edge condition at unloaded edges, a comparison was made in terms of the in-plane displacement as shown in Figure 20. It is obvious from Figure 20 that the in-plane displacement was allowed for the non-straight condition at unloaded edges, but the difference is very small and can be neglected. In fact, the computed results of the ANSYS finite element method in Figure 19 show identical despite the edge straight condition. Figure 21 shows the deformed shape of the plate panel with $t = t_1 = t_2$ = 10 mm at the ultimate limit state obtained from the ANSYS finite element method analysis. The deformed shape of the plate panel observed by the ANSYS analysis is comparable with that by the experiment as shown in Figure 22 where the panel reached the ultimate limit state by collapse mode V (tripping of the stiffeners), although the ANSYS computations did not show a clear tripping failure.

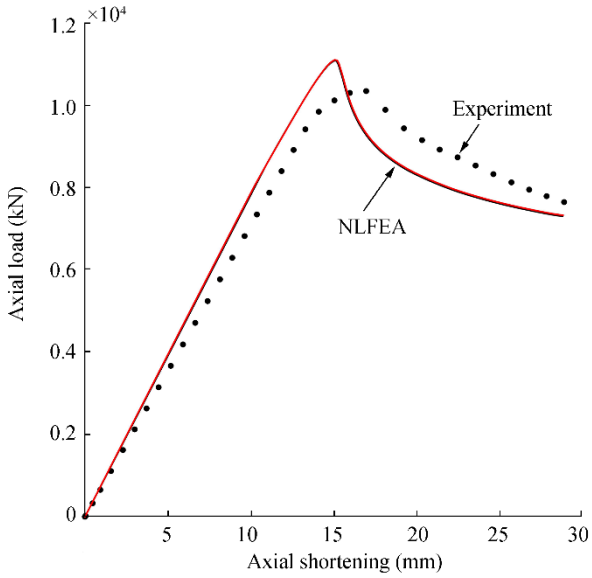

(a) Axial load-axial shortening curve

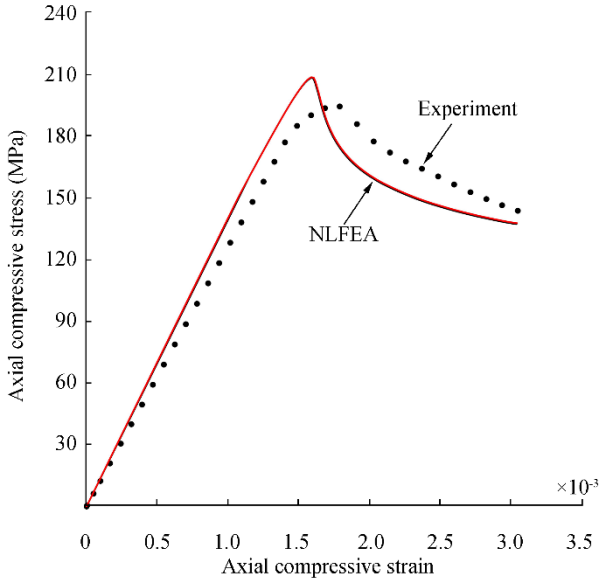

(b) Axial compressive stress-axial compressive strain curve

Figure 19 Comparison of the ultimate compressive strength behaviour of the plate panel between the experiment and ANSYS finite element method analysis

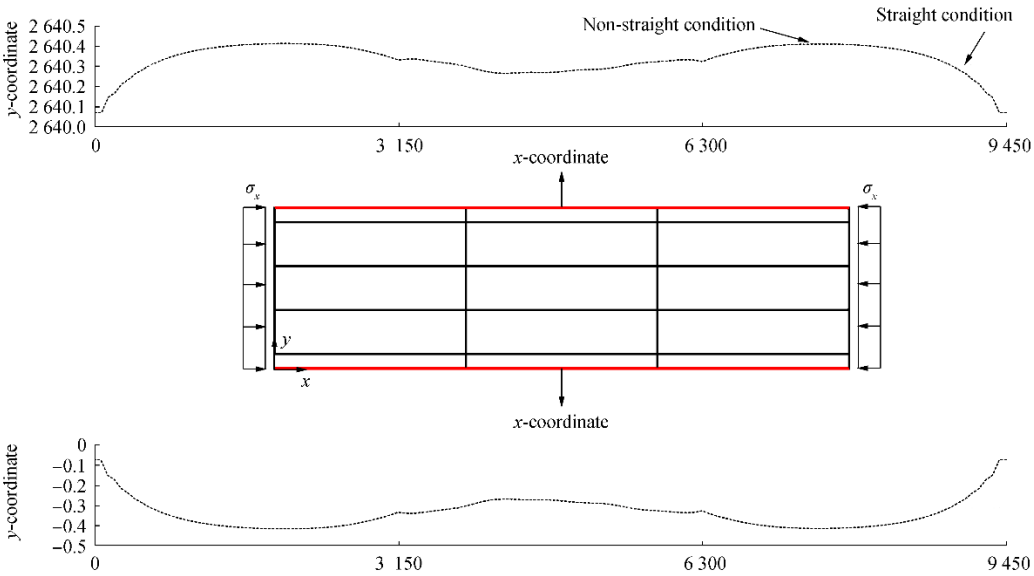

Figure 20 Effects of the straight condition at unloaded edges in terms of the inplane displacement

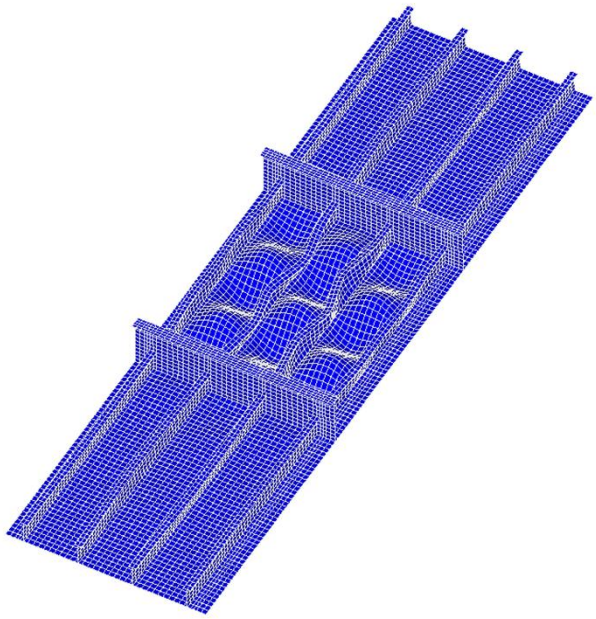

Figure 21 Deformed shape of the plate panel at the ultimate limit state obtained from the ANSYS finite element method analysis (with an amplification factor of 20)

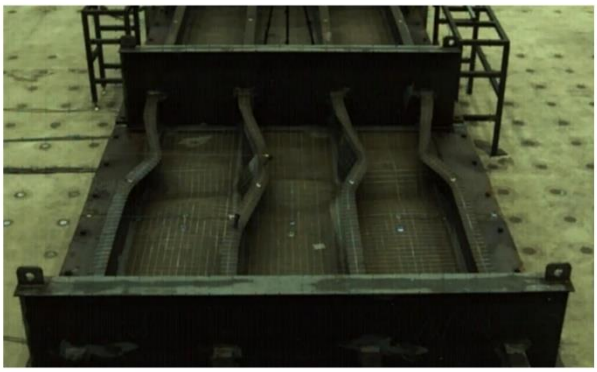

Figure 22 Deformed shape of the plate panel at the ultimate limit state observed from the experiment (Paik et al. 2020a)

To examine the effects of non-uniform thickness on the plate ultimate compressive strength, a series analyses were conducted with varying the plate thickness as indicated in Table 4, where the average value of the plate thickness is the same as 10 mm. Figure 23 shows the ultimate compressive strength behaviour of the plate panel obtained from the ANSYS finite element method analysis with varying the plate thickness. Figure 24 shows the ALPS/SPINE analysis results in terms of added deflection components until the ultimate strength is reached with varying the plate thickness. It is interesting to see that the global pattern of the plate deflection increases in the beginning as the axial compressive loads are increased, but it eventually decreases (and disappears) as the plate buckles so that the buckling mode becomes dominant.

The ALPS/ULSAP predictions were also carried out, and they showed that the panels of the four cases all reached the ultimate limit state by the tripping failure (collapse mode V). Table 5 summarizes the ultimate strength computations together with the experimental result. Figure 25 compares the ultimate compressive strengths obtained from the case studies. The ultimate strength obtained by ANSYS is greater than the experiment by 7.2 % for case 1 with $t = t_1 = t_2$ = 10 mm. It is found that the ANSYS ultimate compressive strength computations of the plate panel with non-uniform thickness decrease as the lower plate thickness t_2 decreases. For case 4 with a thickness difference of $t_1 - t_2$ = 3 mm, the reduction ratio of the ANSYS ultimate strength computation is 16.1%.

On the other hand, the analytical solutions for case 1 are smaller than the experiment by 3.2% for the ALPS/ULSAP analysis and 6.6% for the ALPS/SPINE analysis. By comparing with case 1 and case 4, the reduction rate of the ultimate strength is 3.3% for the ALPS/ULSAP analysis and 6.3% for the ALPS/SPINE analysis. It is obvious that the analytical solution of the panel ultimate strength decreases as the lower thickness decreases but the reduction rate is much small in contrast to the ANSYS computations.

Based on the case studies, it is considered that the average thickness, i.e., $t_{eq} = \frac{t_1 + t_2}{2}$ can approximately be used for the analytical approaches (e.g., ALPS/ULSAP or ALPS/SPINE) of plate panels with non-uniform thickness. The nonlinear finite

element method can of course account for actual thicknesses directly.

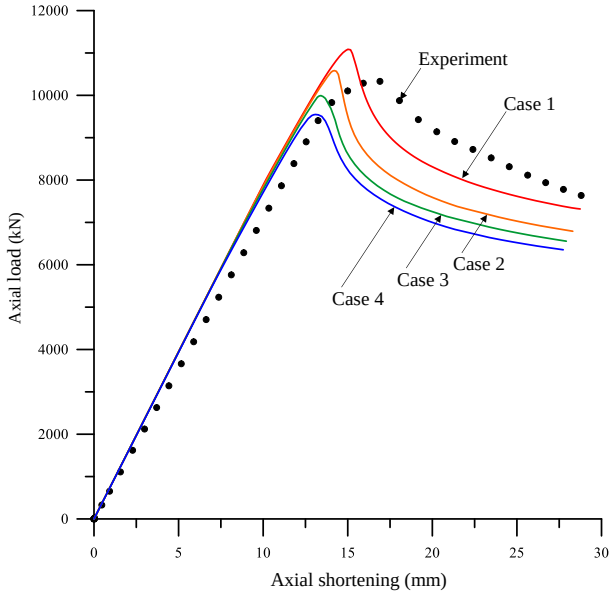

(a) Axial load-axial shortening curve

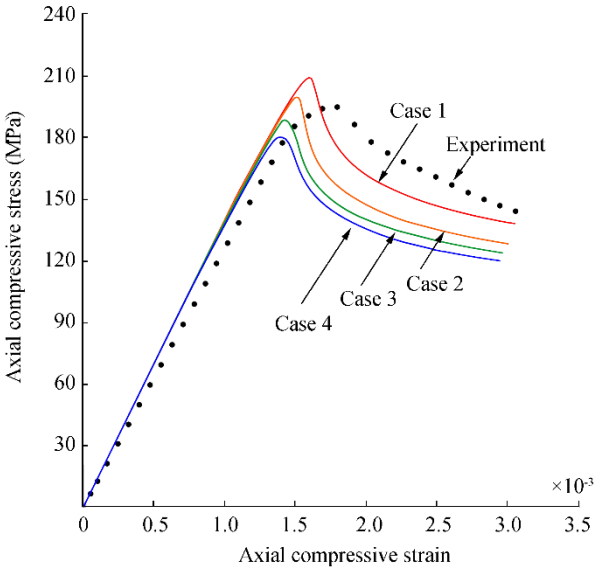

(b) Axial compressive stress-axial compressive strain curve

Figure 23 The ultimate compressive strength behaviour of the plate panel obtained from the ANSYS finite element method analysis

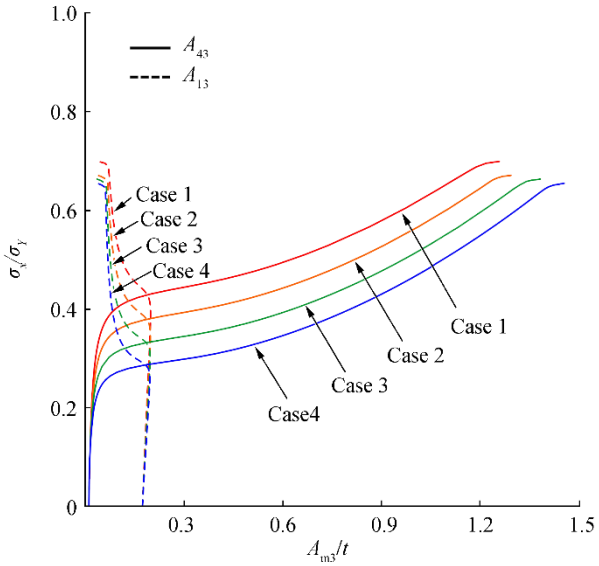

Figure 24 The ALPS/SPINE ultimate compressive strength behaviour of the plate panel in terms of the added deflection components

Table 5 Comparison of the ultimate compressive strength of the plate panels between the three method predictions together with the experiment

Case	Experiment (MPa)	ANSYS[1)] (MPa)	ALPS/ULSAP[2)] (MPa)	ALPS/SPINE[2)] (MPa)
1	248.6	266.5	240.6	232.1
2	-	254.4	237.5	222.7
3	-	240.2	234.8	220.2
4	-	229.5	232.7	217.4

Notes: 1) Actual t_1 and t_2 were applied; 2) $t_{eq}=t_2$ (lower thickness) was applied.

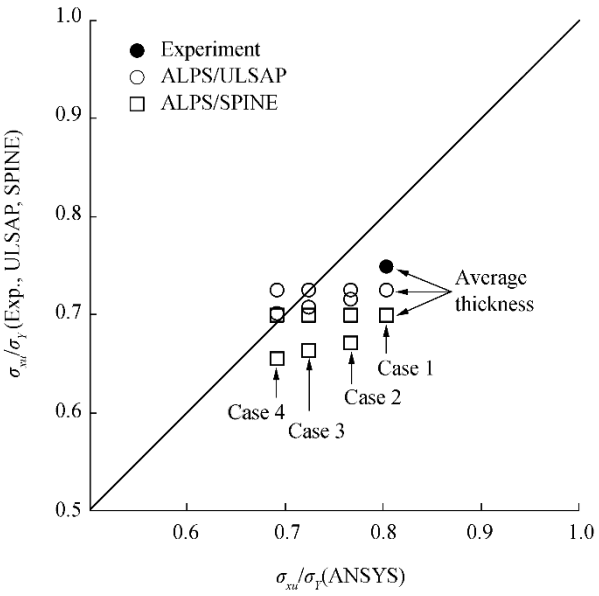

Figure 25 Comparison of the ultimate compressive strength between the analyses and the experiment for the plate panel with varying the thickness

6 Concluding remarks

The aim of the paper was to investigate the effects of non-uniform thickness on the ultimate compressive strength of plate panels so that a recommended practice for defining a representative (equivalent) plate thickness was developed. Case studies were conducted by varying the plate thickness. Based on the studies, the following conclusions can be drawn.

1) The modelling techniques of welding-induced initial deflections and residual stresses in plate panels were presented in association with the measure data.

2) The ANSYS ultimate compressive strength computation for the plate panel with a uniform thickness of 10 mm (case 1) was greater than the experiment by 7.2%.

3) The ALPS/ULSAP or ALPS/SPINE ultimate compressive strength solutions for the plate panel of case 1 were smaller than the experiment by 3.2% and 6.6%, respectively.

4) According to the ANSYS computations, the ultimate compressive strength of plate panels with non-uniform thickness decreases as the lower thickness decreases or the thickness difference increases as far as the average thickness is kept constant.

5) The ALPS/ULSAP predictions showed that the plate panels of the four cases all reached the ultimate limit state triggered by tripping of the longitudinal stiffeners. This corresponds to the panel collapse mode of case 1 by the experiment.

6) The ALPS/ULSAP and ALPS/SPINE solutions show a similar trend to the ANSYS finite element method computations, but the reduction rate of the ultimate compressive strength is much smaller.

7) It is concluded that the average thickness for plate panels with non-uniform thickness can approximately be used as a representative for the ultimate compressive strength analysis by analytical methods which model the plate panels with uniform thickness.

References

Abdussamie N, Ojeda R, Daboos M (2018) ANFIS method for ultimate strength prediction of unstiffened plates with pitting corrosion. Ships and Offshore Structures, **13**(5): 540-550

ALPS/SPINE (2020) Elastic-plastic large deflection analysis of plates and stiffened pan els under combined biaxial compression / tension, biaxial in-plane bending, edge shear and lateral pressure loads. MAESTRO Marine LLC, Greenboro, MD, USA, https://www.maestromarine.com.

ALPS/ULSAP (2020) Ultimate strength analysis of plates and stiffened panels under combined biaxial compression / tension, edge shear and lateral loads. MAESTRO Marine LLC, Greenboro, MD, USA, https://www.maestromarine.com.

ANSYS (2019) User's manual (Version 10.0), ANSYS Inc., Canonsburg, PA, USA.

ASTM (2011) ASTM E8/E8M-09 Standard test methods for tension testing of metallic materials, PA, USA: American Association State International.

Benson S, Downes J, Dow RS (2011) Ultimate strength characteristics of aluminium plates for high-speed vessels. Ships and Offshore Structures, **6**(1-2): 67-80

de Faria AR, de Almeida SFM (2003) Buckling optimization of plates with variable thickness subjected to nonuniform uncertain loads. International Journal of Solids and Structures, **40**: 3955-3966.

DNVGL (2017) Rules for classification – ships, Part 2 Materials and welding, Chapter 4 Fabrication and testing, Høvik, Norway.

Fletcher CAJ (1984) Computational Galerkin method. Springer-Verlag, New York, USA.

Gannon L, Liu Y, Pegg N, Smith MJ (2013) Effect of three-dimensional welding-induced residual stress and distortion fields on strength and behaviour of flat-bar stiffened panels. Ships and Offshore Structures, **8**(5): 565-578.

Gannon L, Liu Y, Pegg N, Smith MJ (2016) Nonlinear collapse analysis of stiffened plates considering welding-induced residual stress and distorion. Ships and Offshore Structures, **11**(3): 228-244.

Iijima K, Suzaki Y, Fujikubo M (2015) Scaled model tests for the post-ultimate strength collapse behaviour of a ship's hull girder under whipping loads. Ships and Offshore Structures, **10**(1): 31-38.

Jagite G, Bigot F, Derbanne Q, Malenica S, Le Sourne H, de Lauzon J, Cartraud P (2019) Numerical investigation on dynamic ultimate strength of stiffened panels considering real loading scenarios. Ships and Offshore Structures, **14**(suppl): 374-386.

Jagite G, Bigot F, Derbanne Q, Malenica S, Le Sourne H, Cartraud P (2020) A parametric study on the dynamic ultimate strength of a stiffened panel subjected to wave- and whipping-induced stresses. Ships and Offshore Structures. https://doi.org/10.1080/17445302.2020.1790985.

Khan I, Zhang S (2011) Effects of welding-induced residual stress on ultimate strength of plates and stiffened panels. Ships and Offshore Structures, **6**(4): 297-309.

Khedmati MR, Memarian HR, Fadavie M, Zareel MR (2016) Empirical formulations for estimation of ultimate strength of continuous aluminium stiffened plates under combined transverse compression and lateral pressure. Ships and Offshore Structures, **11**(3): 258-277.

Khedmati MR, Pedram M, Rigo P (2014) The effects of geometrical imperfections on the ultimate strength of aluminium stiffened plates subject to combined uniaxial compression and lateral pressure. Ships and Offshore Structures, **9**(1): 88-109.

Kim UN, Choe IH, Paik JK (2009) Buckling and ultimate strength of perforated plate panels subject to axial compression: experimental and numerical investigations with design formulations. Ships and Offshore Structures, **4**(4): 337-361.

Kim DK, Kim SJ, Kim HB, Zhang XM, Li CG, Paik JK (2015) Ultimate strength performance of bulk carriers with various corrosion additions. Ships and Offshore Structures, **10**(1): 59-78.

Kumar MS, Alagusundaramoorthy P, Sundaravadivelu R (2009) Interaction curves for stiffened panel with circular opening under axial and lateral loads. Ships and Offshore Structures, **4**(2): 133-143.

Lee DH, Kim SJ, Lee MS, Paik JK (2019) Ultimate limit state based design versus allowable working stress based design for box girder crane structures. Thin-Walled Structures, **134**: 491-507.

Lee DH, Paik JK (2020) Ultimate strength characterfistics of as-built ultra-large containership hull structures under combined vertical bending and torsion. Ships and Offshore Structures, doi: https://doi.org/10.1080/17445302.2020.1747829.

Le-Manh T, Huynh-Van Q, Phan TD, Phand HD, Nguyen-Xuan H (2017) Isogeometric nonlinear bending and buckling analysis of variable-thickness composite plate structures. Composite Structures, **159**: 818-826.

Magoga T, Flockhart C (2014) Effect of weld-induced imperfections on the ultimate strength of an aluminium patrol boat determined by the ISFEM rapid assessment method. Ships and Offshore Structures, **9**(2): 218-235.

Ozguc O, Das PK, Barltrop N (2006) A proposed method to evaluate hull girder ultimate strength. Ships and Offshore Structures, **1**(4): 335-345.

Paik JK (2007) Ultimate strength of steel plates with a single circular hole under axial compressive loading along short edges. Ships and Offshore Structures, **2**(4): 355-360.

Paik JK (2018) Ultimate limit state analysis and design of plated structures. John Wiley & Sons, Chichester, UK.

Paik JK (2020) Advanced structural safety studies with extreme conditions and accidents. Springer, Singapore.

Paik JK, Kim DK, Park DH, Kim HB, Mansour AE, Caldwell JB (2013) Modified Paik-Mansour formular for ultimate strength calculations of ship hulls. Ships and Offshore Structures, **8**(3-4): 245-260.

Paik JK, Lee MS (2005) A semi-analytical method for the elastic-plastic large deflection analysis of stiffened panels under combined biaxial compression/tension, biaxial in-plane bending, edge shear and lateral pressure loads. Thin-Walled Structures, **43**(2): 375-410.

Paik JK, Lee DH, Noh SH, Park DK, Ringsberg JW (2020a) Full-scale collapse testing of a steel stiffened plate structure under cyclic axial-compressive loading. Structures, **26**: 996-1009.

Paik JK, Lee DH, Noh SH, Park DK, Ringsberg JW (2020b) Full-scale collapse testing of a steel stiffened plate structure under axial-compressive loads triggered by brittle fracture at cryogenic condition. Ships and Offshore Structures. https://doi.org/10.1080/17445302.2020.1787930

Paik JK, Lee DH, Noh SH, Park DK, Ringsberg JW (2020c) Full-scale collapse testing of a steel stiffened plate structure under axial-compressive loads at temperature of -80℃. Ships and Offshore Structures. https://doi.org/10.1080/17445302.2020.1791685.

Paik JK, Ryu MG, He K, Lee DH, Lee SY, Park DK, Thomas G (2020d) Full-scale fire testing to collapse of steel stiffened plate structures under lateral patch loading (part 1) – without passive fire protection. Ships and Offshore Structures. https://doi.org/10.1080/17445302.2020.1764705.

Paik JK, Ryu MG, He K, Lee DH, Lee SY, Park DK, Thomas G. (2020e) Full-scale fire testing to collapse of steel stiffened plate structures under lateral patch loading (part 2) – with passive fire protection. Ships and Offshore Structures. https://doi.org/10.1080/17445302.2020.1764706.

Paik JK, Thayamballi AK, Lee SK, Kang SJ (2001) A semi-analytical method for the elastic-plastic large deflection analysis of welded steel or aluminum plating under combined in-plane and lateral pressure loads. Thin-Walled Structures, **39**: 125-152.

Rahbar-Ranji A, Zarookoan A (2015) Ultimate stregth of stiffened plates with a transverse crack under uniaxial compression. Ships and Offshore Structures, **10**(4): 416-425.

Ringsberg JW, Li Z, Johnson E, Kuznecovs A, Shafieisabet R (2018) Reduction in ultimate strength capacity of corroded ships involved in collision accidents. Ships and Offshore Structures, **13**(sup1): 155-166.

Shi G, Gao D (2020) Ultimate strength of U-type stiffened panels for hatch covers used in ship cargo holds. Ships and Offshore Structures. https://doi.org/10.1080/17445302.2020.1724359.

Shi G, Wang D (2012) Ultimate strength model experiment regarding a container ship's hull structures. Ships and Offshore Structures, **7**(2): 165-184.

Tash FY, Neya BN (2020) An analytical solution for bending of transversely isotropic thick rectangular plates with variable thickness. Applied Mathematical Modelling, **77**: 1582-1602.

Yi MS, Lee DH, Lee HH, Paik JK (2020a) Direct measurements and numerical predictions of welding-induced initial deformations in a full-scale steel stiffened plate structure. Thin-Walled Structures. https://doi.org/10.1016/j.tws.2020.106786.

Yi MS, Noh SH, Lee DH, Seo DH, Paik JK (2020b) Direct measurements, numerical predictions and simple formula estimations of welding-induced biaxial residual stresses in a full-scale steel stiffened plate structure. Structures. https://doi.org/10.1016/j.istruc.2020.05.030

Zhang S (2016) A review and study on ultimate strength of steel plates and stiffened panels in axial compression. Ships and Offshore Structures, **11**(1): 81-91.

Zhang J, Hua Z, Tang W, Wang F, Wang S (2018) Buckling of externally pressurised egg-shaped shells with variable and constant wall thickness. Thin-Walled Structures, **132**: 111-119.

Zenkour AM (2003) An exact solution for the bending of thin rectangular plates with uniform, linear, and quadratic thickness variations. International Journal of Mechanical Sciences, **45**: 295-315.

Wang G, Sun H, Peng H, Uemori R (2009) Buckling and ultimate strength of plates with openings. Ships and Offshore Structures, **4**(1): 43-53.